ARTIFICIAL TRANSMISSION LINE WITH LEFT/RIGHT-HANDED BEHAVIOR BASED ON WIRE BONDED INTERDIGITAL CAPACITORS

J. J. Sánchez-Martínez, E. Márquez-Segura, P. Otero and C. Camacho-Peñalosa

Dpt. Ingeniería de Comunicaciones
E. T. S. Ingeniería de Telecomunicación
Universidad de Málaga
Málaga 29071, Spain

Abstract—A novel artificial transmission line with right/left-handed behavior is presented in this paper. The unit cell of the new artificial line consists of one series and one shunt wire bonded interdigital capacitors. When wire bonded interdigital capacitors are used, the artificial line has a wider frequency band of operation. A combined analytical-graphical design method of the proposed artificial transmission line is also presented. The method has been assessed with the help of an electromagnetic solver based on the method of moments, and experimental work.

1. INTRODUCTION

Last year's artificial transmission line structures that simulate the behavior of materials with negative values of electric permittivity, ϵ, and magnetic permeability, μ (left-handed materials) have focused the attention of numerous engineers [1, 2]. These structures have established the basis for the development of new applications of passive and active devices in microwave engineering. Nevertheless, left-handed materials are not found in nature. Several structures have been presented that emulate mediums with $\epsilon < 0$ and $\mu < 0$ [3, 4]. Metamaterials based on resonant elements present large losses and narrow frequency bands that limit their application in microwave engineering. Left-handed artificial transmission lines partially overcome these problems because they do not use resonant devices, so losses are smaller and the operating frequency band is wider [5–7]. A left-handed transmission line can be simulated by

cascading cells like the one shown in Fig. 1(a), which is the dual circuit of the single cell of a conventional transmission line, shown in Fig. 1(b). However, when doing so, the parasitic effects of the capacitors and the inductor of the circuit in Fig. 1(b) result in a combined behavior, the so-called composite right/left-handed transmission lines, (CRLH) [7].
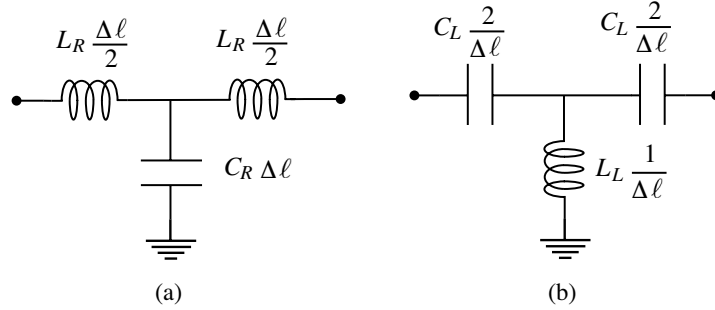

(a)   (b)

Figure 1. Equivalent circuits of a short transmission line ($\beta \triangle \ell \ll 1$). (a) Right-handed LC equivalent circuit. (b) Left-handed CL equivalent circuit.
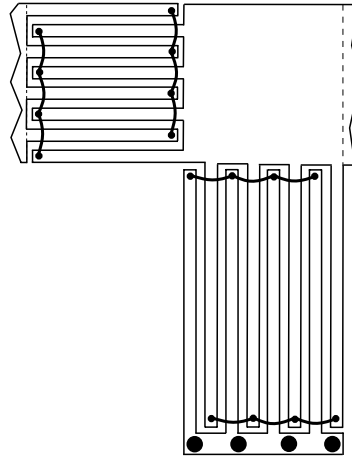

Figure 2. Unit-cell of the composite right/left handed transmission line using two wire bonded interdigital capacitors.

In this paper a transmission line cell that consists of two wire bonded interdigital capacitors is presented, as is shown in Fig. 2. The line that can be built by cascading these cells shows better behavior as an artificial transmission line with left-handed behaviour. This

artificial line is very convenient for integration in planar technology. The use of wire bonded interdigital capacitor eliminates the resonances due to the multiconductor nature of the interdigital capacitor [7–9]. Section 2 contains the theoretical analysis of the line, supported by electromagnetic simulation based on the method of moments. Section 3 deals with the actual behavior of the line when the parasitic effects of the interdigital capacitors are taken into account. In Section 4, the results of several experiments are shown, to demonstrate the validity of the previous analysis and the design method.

2. RIGHT/LEFT-HANDED STRUCTURE BASED ON INTERDIGITAL CAPACITORS

A cell with similar behavior to that of the circuit shown in Fig. 1(b) can be built in microstrip technology using only interdigital capacitors. The shunt inductance can be also implemented by means of an interdigital capacitor, operating at a frequency where it is no longer a capacitor, but an inductor. The purpose of this Section is to design the capacitors for the artificial line to show the desired left-handed behavior over a specified frequency band.

2.1. The Wire Bonded Interdigital Capacitor

The wire bonded interdigital capacitor is an improved interdigital capacitor without the undesired resonances at higher frequencies due to its multi-conductor structure [8]. The improvement is easily obtained using bonding wires across the end of alternate fingers. The conventional capacitor and the wire bonded capacitor are shown in Fig. 3. The latter is needed to build left-handed lines, instead of the former, because it has to operate at the extended frequency range where the conventional capacitor is no longer useful due to the
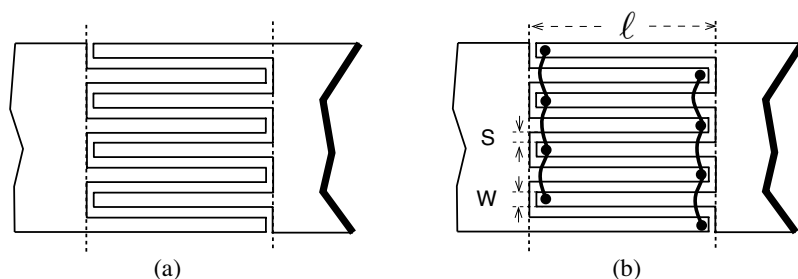

Figure 3. (a) Interdigital capacitor. (b) Wire bonded interdigital capacitor.

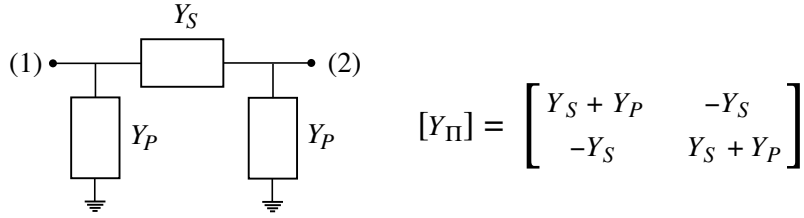$$[Y_\Pi] = \begin{bmatrix} Y_S + Y_P & -Y_S \\ -Y_S & Y_S + Y_P \end{bmatrix}$$

Figure 4. Admittance matrix of a network. This network is the equivalent circuit of the wire bonded interdigital capacitor of Fig. 3(b).

undesired resonances. Fig. 4 shows the equivalent $\prod$ circuit of the wire bonded interdigital capacitor of Fig. 3(b). Beyond frequency f_{s1}, which is the lowest pole of the admittance Y_S, the device has a positive reactance [9]. The admittance matrix of the wire bonded interdigital capacitor is

$$[Y_W] = \frac{j\left(M^2 - N^2\right)\sin\theta}{M^2\cos^2\theta - N^2} \begin{bmatrix} M\cos\theta & N \\ N & M\cos\theta \end{bmatrix} \tag{1}$$

where θ is the electrical length of the capacitor fingers, i.e., $\theta = \beta\ell$, where β is the phase constant of the multiconductor structure, and ℓ is finger length. The value of β is obtained from the effective permittivity of a pair of coupled lines, as explained in [9, 10]. The quantities M and N are given by

$$M = \frac{n}{2}Y_{11} + \left(\frac{n}{2} - 1\right)\frac{Y_{12}^2}{Y_{11}} \tag{2}$$

$$N = (n-1)Y_{12}, \tag{3}$$

where n is the number of fingers and Y_{11} and Y_{12} are

$$Y_{11} = \frac{1}{2}\left(Y_{oo} + Y_{oe}\right) \tag{4}$$

$$Y_{12} = -\frac{1}{2}\left(Y_{oo} - Y_{oe}\right) \tag{5}$$

The admittances Y_{oe} and Y_{oo}, which are the even and odd mode characteristic admittances, respectively, of a pair of equivalent coupled lines [9, 10], depend on the transversal dimensions of the capacitor. The admittances Y_S and Y_P of Fig. 4, therefore, are

$$Y_S = j\frac{N\left(N^2 - M^2\right)\sin\theta}{M^2\cos^2\theta - N^2} \tag{6}$$

$$Y_P = -j\frac{(N^2 - M^2)\sin\theta}{M\cos\theta - N} \qquad (7)$$

At low frequencies both Y_S and Y_P are capacitive admittances. At higher frequencies they turn into inductive admittances. The poles and zeros in Eqs. (6) and (7) determine the frequency response of the capacitor.

2.2. Asymmetric Unit Cell

An artificial left-handed transmission line can be designed by cascading single two-port cells, with each cell consisting of two wire bonded interdigital capacitors, one in series, one shunted to ground (Fig. 2). The circuit model of the cell is obtained using the Π circuit model of the wire bonded capacitor (Fig. 5). The phase shift of the single cell must be small so that it can be considered a short length of the equivalent transmission line. When several cells are cascaded, the characteristic impedance, Z_0, and the propagation constant, γ, of the artificial line can be calculated from the equivalent circuit, which is shown in Fig. 6.
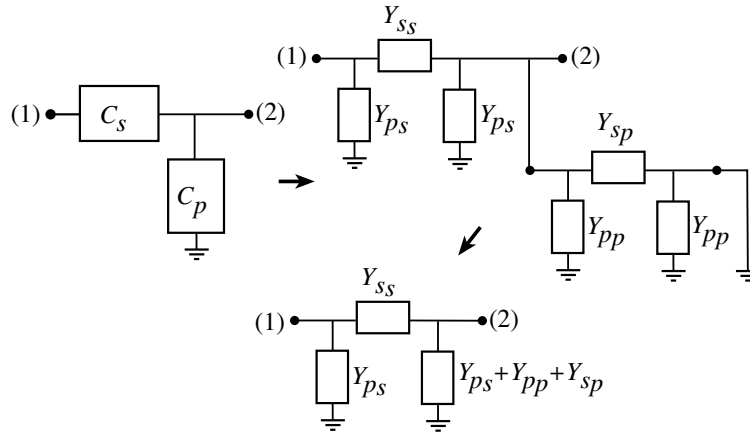

Figure 5. Equivalent circuit of the cell that uses the admittances of the analytical model. C_S and C_P stand for series and parallel capacitors, respectively.

In Fig. 6, $Y_{Px} = Y_{Ps} + Y_{Pp} + Y_{Sp}$, therefore

$$Z = \frac{1}{Y_{s_s}} = j\frac{M_s^2\cos^2\theta_s - N_s^2}{N_S(M_s^2 - N_s^2)\sin\theta_s} \qquad (8)$$

$$Y = 2Y_{p_s} + Y_{p_p} + Y_{s_p}$$

$$= -j \left(\frac{2\left(N_s^2 - M_s^2\right)\sin\theta_s}{M_s \cos\theta_s - N_s} + \frac{M_p\left(N_p^2 - M_p^2\right)\sin(2\theta_p)}{2\left(M_p^2 \cos^2\theta_p^2 - N_p^2\right)} \right) \quad (9)$$

If both capacitors of the cell are equal, with the exception of their lengths, then $M_s = M_p = M$ and $N_s = N_p = N$ and (8) and (9) become

$$Z = j\frac{M^2 \cos^2\theta_s - N^2}{N\left(M^2 - N^2\right)\sin\theta_s} \quad (10)$$

$$Y = j\left(M^2 - N^2\right)\left(\frac{2\sin\theta_s}{M\cos\theta_s - N} + \frac{M\sin(2\theta_p)}{2(M^2\cos^2\theta_p - N^2)}\right) \quad (11)$$

The characteristic impedance and the propagation constant of the artificial line are given by

$$Z_o = \sqrt{\frac{Z}{Y}} \quad (12)$$

$$\gamma\Delta\ell = \sqrt{ZY} \quad (13)$$

where $\Delta\ell$ is the length of the cell.

Both capacitors of Fig. 2 have to be designed to operate at the transition frequency (f_o), which is the frequency where the value of the phase constant of the artificial transmission line changes from negative to positive. Once the substrate is defined, four geometrical parameters
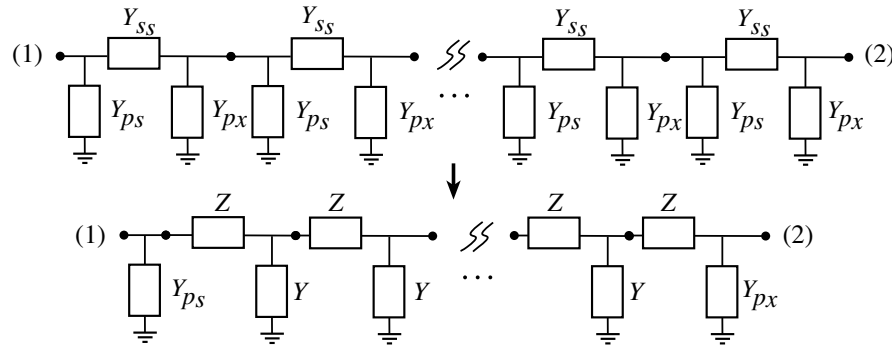

Figure 6. Right/left handed artificial transmission line cascading several unit cells.

characterize a wire bonded interdigital capacitor, namely the number of fingers, the width and length of the fingers, and the finger spacing. However, it is common practice to choose the width of the capacitor equal to the width of a microstrip line with characteristic impedance equal to the reference impedance, which in our case is $50\,\Omega$.
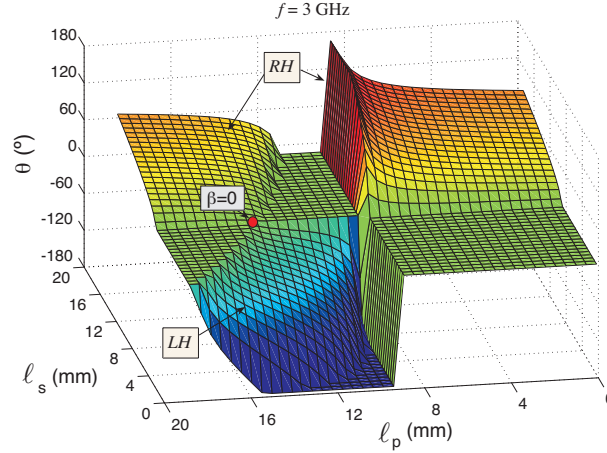

Figure 7. Electrical length, $\theta = \beta\ell$, of a lossless cell, in a three-dimensional view. ℓ_p and ℓ_s are the physical lengths of the shunt and series wire bonded interdigital capacitors of Fig. 2, respectively. (RH stands for right-handed and LH stands for left-handed).

For two given capacitors operating at a given frequency, once the number of fingers and their widths and separations have been designed, it is possible to calculate the phase shift introduced by a cell as a function of their finger lengths. Fig. 7 shows one example, where the capacitors have been designed on a lossless substrate with relative permittivity $\epsilon_r = 2.4$, thickness $h = 1.57\,\text{mm}$, with eight fingers of $350\,\mu\text{m}$ wide and separations of $270\,\mu\text{m}$. Fig. 8 shows the same function using a color code instead of a spatial surface. Figs. 7 and 8 show clearly the different behaviors of the artificial lines that can be designed and built. There is a single point where $\beta = 0$ and this is shown in Fig. 7 and Fig. 8.

When losses are not taken into account, Z and Y are pure imaginary. Fig. 9 shows the values of Z and Y vs. frequency and, therefore, the behavior of the artificial line. Below a frequency, which in our example is around $2\,\text{GHz}$, both capacitors are capacitances, the propagation constant is real and there is no propagation. Above this value, the shunt capacitor has a positive reactance, the propagation

constant is pure imaginary and the characteristic impedance is real. The value of Z_0 is between $26\,\Omega$ and $96\,\Omega$ in the frequency range, which means that the matching is better than $-10\,\text{dB}$. Thus, the method developed above offers a graphical tool to find the finger lengths of the wire bonded interdigital capacitors for the transition frequency to be a given value, and still have a good matching. For instance, Fig. 8 shows that, if $f_o = 3\,\text{GHz}$ is desired, the lengths of the series and shunt capacitors will be $9.23\,\text{mm}$ and $13.98\,\text{mm}$, respectively. Moreover, Fig. 9 shows that the artificial line is always balanced, since the left-handed/right-handed transition occurs at a single frequency, without a gap.
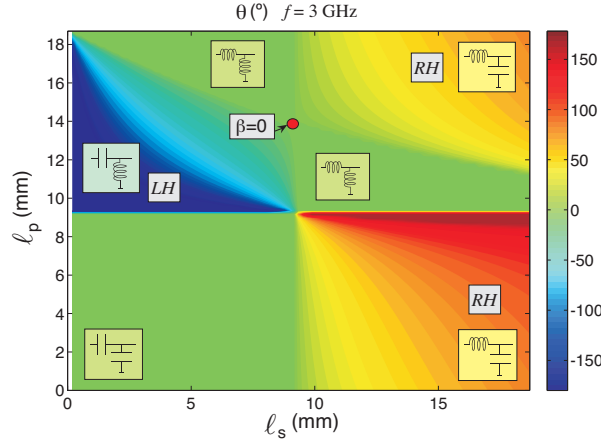

Figure 8. Electrical length, $\theta = \beta\ell$, of a lossless cell, in a planar view. ℓ_p and ℓ_s are the physical lengths of the shunt and series wire bonded interdigital capacitors of Fig. 2, respectively. (RH stands for right-handed and LH stands for left-handed).

Graphical solution is not the only choice, because analytical expressions for Z and Y are available, as shown in Section 2.1. The finger length of the series capacitor can be calculated as

$$\ell_s = \frac{c}{2\pi f \sqrt{\epsilon_{r_{eff}}}} \arccos\left(\frac{N}{M}\right), \tag{14}$$

where c is the speed of light and $\epsilon_{r_{eff}}$ the effective relative permittivity [9] Once the series capacitor has been designed, the finger length of the shunt capacitor has to be calculated so that the first zero of its
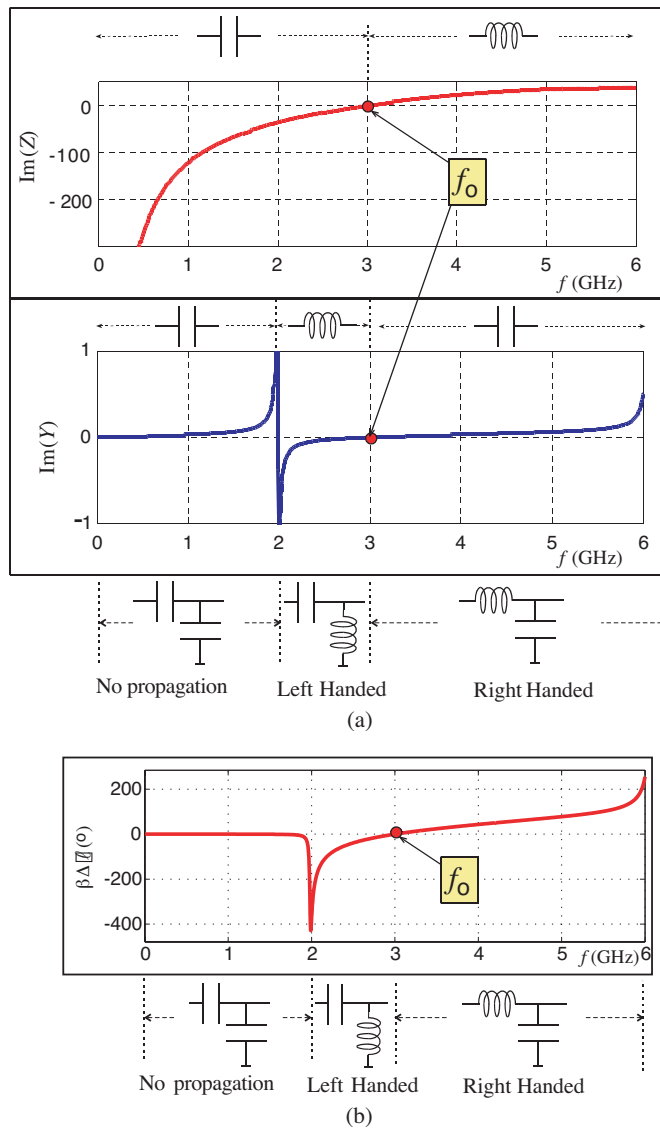
Figure 9. (a) Values of Z and Y of Fig. 6, and cell behavior. (b) $\beta\Delta\ell$ of the unit cell.

admittance also occurs at f_o, which results in

$$
\ell_p = \frac{c}{2\pi f \sqrt{\epsilon_{r_{eff}}}} \arctan \left(\frac{-M \left(M \cos \theta_s - N \right)}{-4 \, N^2 \sin \theta_s} \right.
$$
$$
\left. + \frac{\sqrt{16 \, N^2 \sin^2 \theta_s (M^2 - N^2) + M^2 (M \cos \theta_s - N)^2}}{-4 \, N^2 \sin \theta_s} \right) \quad (15)
$$

The calculated lengths using (14) and (15) are 9.2 mm and 14.0 mm for the series and the shunt capacitors, respectively, which concur with the values obtained from Fig. 8. It is very important to note that the solution for ℓ_p and ℓ_s is unique and therefore the structure is balanced, as mentioned above.
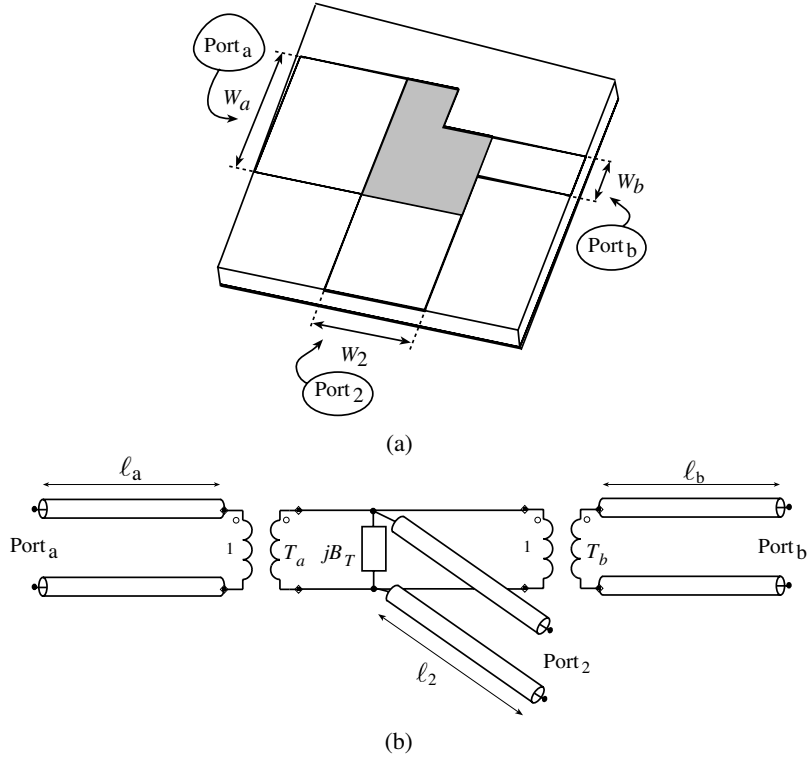

Figure 10. (a) Asymmetric microstrip tee junction. (b) Equivalent circuit.

3. PARASITIC EFFECTS IN THE STRUCTURE

ADS-Momentum has been used to assess the validity of (10) and (11) for Z and Y, respectively. Frequency offsets larger than 18% were obtained between the results obtained using (10)–(11) and the results of Momentum. This discrepancy is because the analytical method obviates, first, the microstrip tee-junction used to connect the two capacitors and to cascade the cells, and second, the via holes of the shunt capacitors.
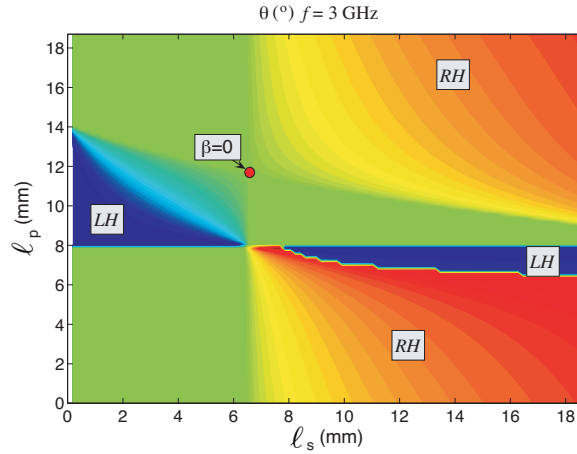

Figure 11. Electric length of the cell when the parasitic effects are taken into account (RH stands for right-handed and LH stands for left-handed).

The via hole can be modeled with a resistance and a series inductance [11]. Special attention must be paid to the microstrip tee junction. Previous work is extensive [12–17], but exact models exist only for low frequency, and for junctions with the same characteristic impedance in all the three ports. After several trials, the model in [17] (Fig. 10), which is also the model used in ADS, has been preferred to others. Fig. 10 represents an asymmetric microstrip tee junction where the main and side arms are denoted by Port a, Port b, and Port 2 respectively. Nevertheless, a slight correction has been added to the chosen model in the following way

$$\ell_{a,b} = 0.723 \cdot W_2 - d_{a,b} \tag{16}$$
$$\ell_2 = 0.98 \cdot \max\left(W_a, W_b\right) - d_2 \tag{17}$$

where $d_{a,b}$ and d_2 are the main and side arm offsets of the reference

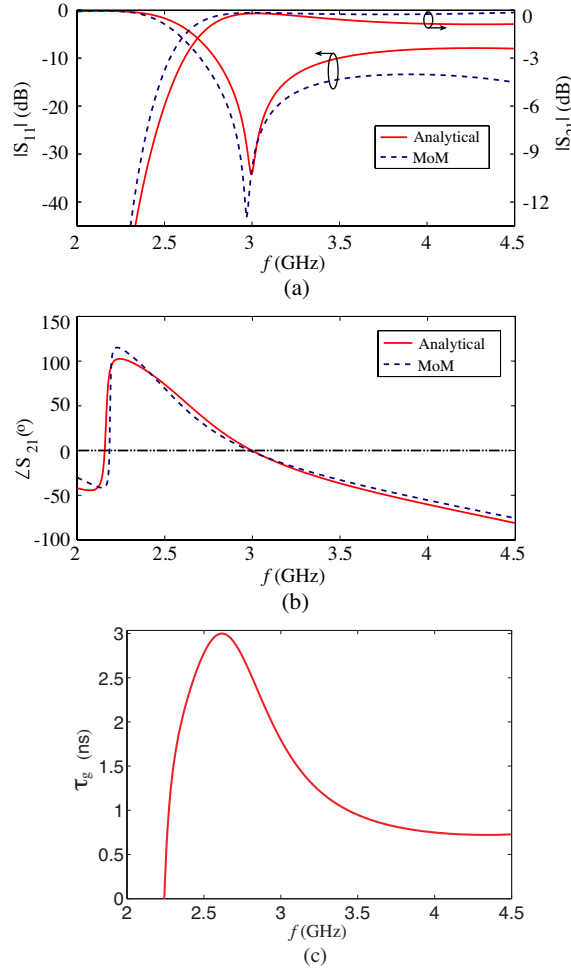**Figure 12.** Analytical and simulated scattering matrix elements and group delay of the cell with the modified tee included ($f_o = 3\,\mathrm{GHz}$).

planes from the center lines. Eqs. (16) and (17) in [17] have a similar factor of 0.5 instead of 0.723 and 0.98. The new factors have been obtained by comparing electromagnetic simulations and scattering parameters calculated with the equivalent circuit shown in Fig. 10(b). This model is useful as long as the physical dimensions of the T-junction are not changed.

When the above mentioned model is used, only the graphical method of Section 2.2 is possible. Fig. 8 becomes Fig. 11 when the parasitic effects of the junction and the via-holes are taken into account.

Fig. 11 is similar to Fig. 8, with the exception of a small shift of the transition frequency f_o to shorter capacitors. With the help of Fig. 11, the lengths of the fingers of the series and shunt capacitors must be 6.48 mm and 11.60 mm, respectively.

Again, in order to assess the design method, a number of analyses with Momentum-ADS at $f_o = 3$ GHz and $f_o = 4$ GHz were carried out. The physical dimensions of the four capacitors used are shown in Table 1. Figs. 12 and 13 show the scattering matrix elements of both cells. The two analysis give very similar results. Table 1 also shows
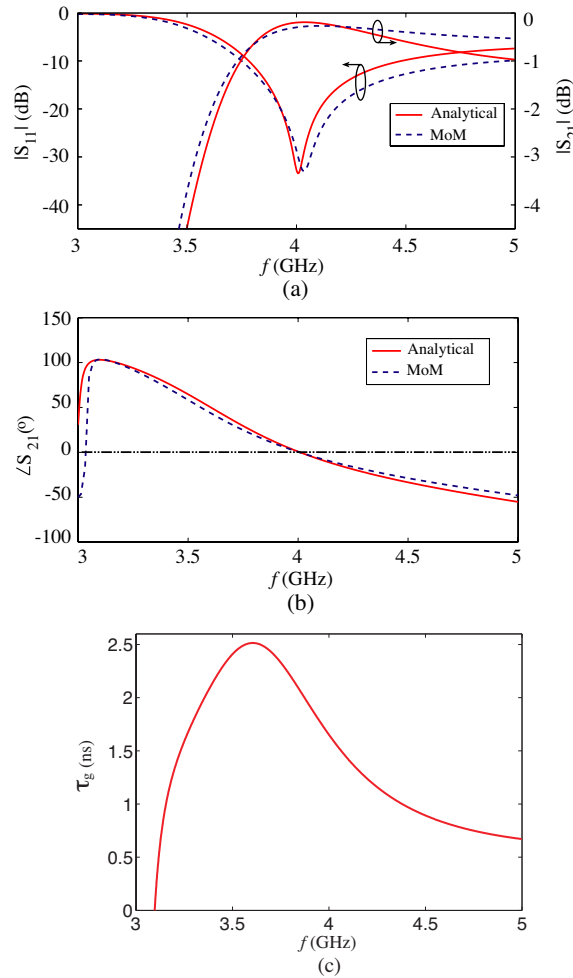

Figure 13. Analytical and simulated scattering matrix elements and group delay of the cell with the modified tee included ($f_o = 4$ GHz).
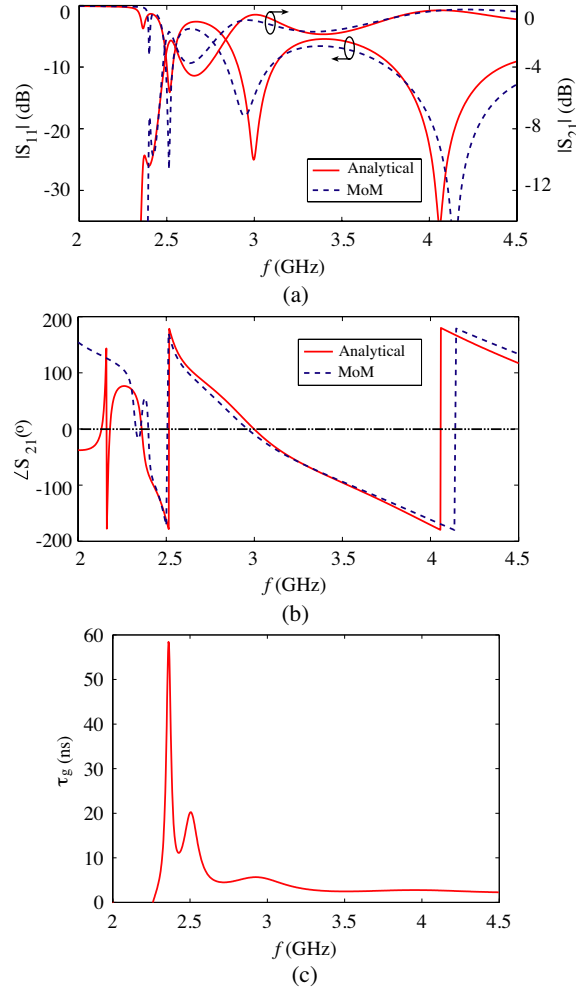
Figure 14. Analytical and simulated scattering matrix elements and group delay of an asymmetric artificial line with three cells ($f_o = 3\,\text{GHz}$).

the transition frequency difference computed in both ways. The error is less than 1% in the two cases. Fig. 14 shows the scattering matrix elements of an artificial line of three cells. Again, the Momentum-ADS results concur with the results of the design method of Section 2. With regards to Fig. 6, it should be mentioned that in the analytical design of the structure the terminal admittance at port 1, Y_{ps}, and the terminal admittance at port 2, Y_{px}, have been neglected, because they
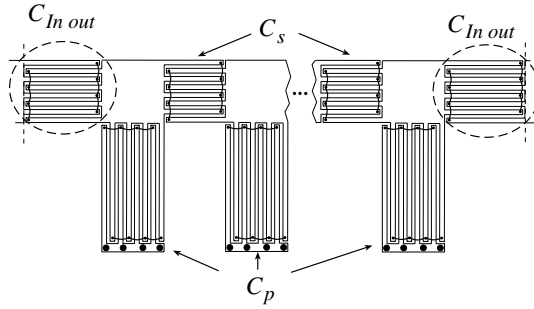
Table 1. ℓ_s and ℓ_p for $f_o = 3$ and $4\,\mathrm{GHz}$.

f_o (GHz)	ℓ_s (mm)	ℓ_p (mm)	f_{o_A}	f_{o_S}	Error (%)
3	6.48	11.6	2.998	2.984	0.46
4	4.17	7.98	4.009	4.007	0.05

are not relevant for the final results.

f_o: Transition frequency (design frequency).

ℓ_s, ℓ_p: Lengths of the series and shunt interdigital capacitors, respectively.

f_{o_A}, f_{o_S}: Analytical and simulated transition frequencies.

Figure 15. Symmetric artificial transmission line using double-value wire bonded interdigital capacitors at both ends.

4. SYMMETRICAL CELL

A section of real line is a symmetric two port network. To improve the behavior of an artificial transmission line, both ends of the line should be equal. Two double-value series capacitors have to be included at the ends of the artificial line, as shown in Fig. 15. The number of fingers and their lengths are changed in order to keep the capacitor width and avoid unnecessary discontinuities. The analytical model of the wire bonded interdigital capacitor can be used for this purpose [9]. To demonstrate the idea, a symmetric line has been designed to operate at $f_o = 3\,\mathrm{GHz}$. The physical dimensions of the wire bonded interdigital capacitors are summarized in Table 2. Fig. 16 shows the scattering matrix elements of the symmetric line with three cells. The symmetric line of Fig. 16 is better matched and presents smaller transmission ripple than the asymmetric line of Fig. 14.

5. EXPERIMENTAL RESULTS

Before building or measuring any prototype, the analytical method was first verified with the help of ADS Momentum. The results of the analytical method fitted the Momentum results. Eventually, a number of experiments were planned and carried out in order to verify the results presented in the previous Sections. Although results are similar in all cases, only two of them are shown here. Two different
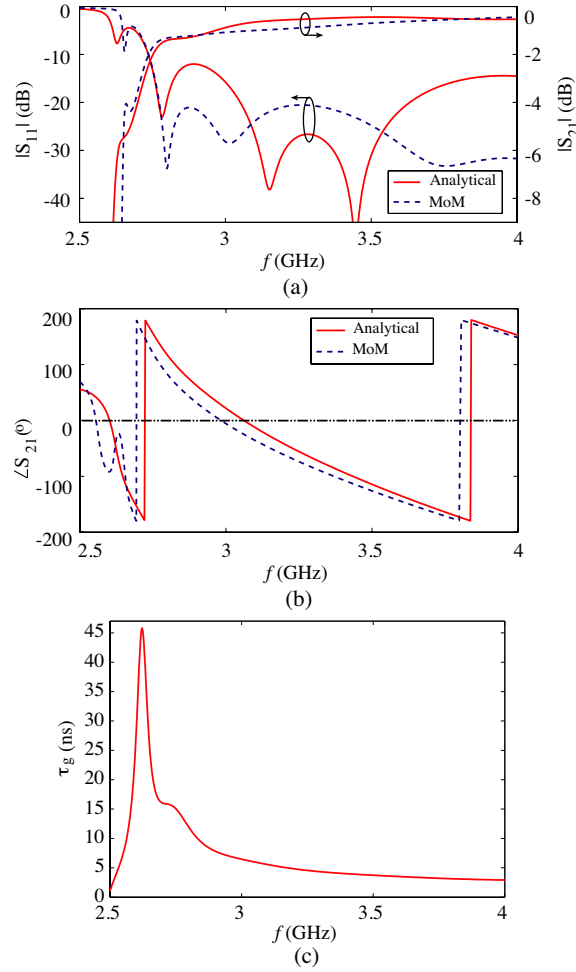

Figure 16. Analytical and simulated scattering matrix elements and group delay of a symmetric artificial line with three cells ($f_o = 3\,\text{GHz}$).

Table 2. Physical lengths of symmetric artificial line with three cells with the topology shown in Fig. 15, $f_o = 3$ GHz.

	$C_{In\ Out}$	C_s	C_p
n	8	8	8
W_d (μm)	350	350	350
S_d (μm)	271.43	271.43	271.43
ℓ (mm)	9	5.64	10.28

n: number of fingers

W_d: width of fingers

S_d: separation between fingers
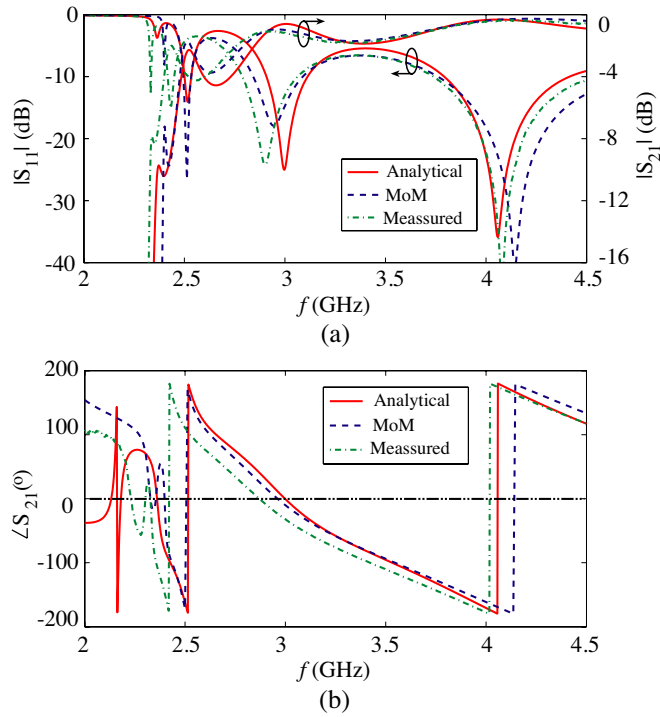
ℓ: length of the fingers

(a)

(b)

Figure 17. Analytical, simulated and measured scattering matrix elements of the artificial line with three cells in asymmetric configuration ($f_o = 3$ GHz).
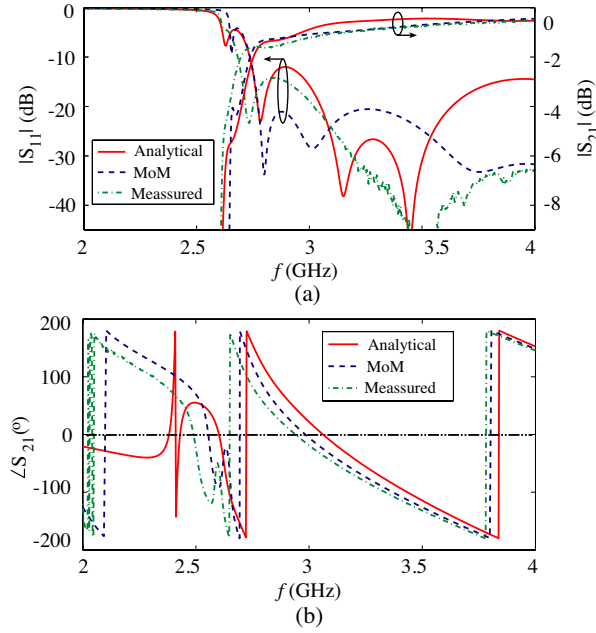
Figure 18. Analytical, simulated and measured scattering matrix
elements of the artificial line with three cells in symmetric configuration
($f_o = 3\,\text{GHz}$).

prototypes were printed on a Rogers Ultralam 2000 substrate, with
relative permittivity of 2.4 and thickness of 1.57 mm. The physical
dimensions of the prototypes are those calculated in Sections 3 and 4
to obtain $f_o = 3\,\text{GHz}$. The first prototype has three cells in asymmetric
configuration. The second prototype is similar, but in symmetric
configuration. Measurement has been carried out by a vector network
analyzer calibrated using the TRL method. Figs. 17 and 18 show the
scattering matrix elements of the two artificial lines. There is also very
good agreement between the predicted and the measured values, in all
cases, which demonstrates the robustness of the design method. The
new method will be of valuable help to integrate this kind of artificial
lines in planar designs.

6. CONCLUSION

A planar structure in microstrip technology has been presented to
synthesize artificial right/left-handed transmission lines. The cell of
the artificial line consists of two wire bonded interdigital capacitors to

achieve both capacitive and inductive behavior. An analytical design method has been developed to design the corresponding transmission lines using the previously presented cells. Artificial lines designed with the proposed method have been validated with numerical simulations using a full-wave electromagnetic solver and experimental work. A remarkable characteristic is that the proposed design method ensures a balanced structure, so there will always be a smooth, continuous transition from left-handed to right-handed propagation regions. It is important to mention that, when used in planar integrated circuits, using this new cell with a shunt interdigital capacitor makes easier to bias the circuits.

ACKNOWLEDGMENT

REFERENCES

1. Caloz, C. and T. Itoh, *Electromagnetic Metamaterials: Tansmission Line Theory and Microwave Applications*, John Wiley & Sons, Inc., Hoboken, NJ, 2006.

2. Eleftheriades, G. V. and K. G. Balmain, *Negative Refraction Metamaterials: Fundamental Principles and Applications*, Wiley-IEEE Press, 2005.

3. Smith, D. R., W. J. Padilla, D. C. Vier, S. C. Nemat-Nasser, and S. Schultz, "Composite medium with simultaneously negative permeability and permittivity," *Phys. Rev. Lett.*, Vol. 84, No. 18, 4184–4187, 2000.

4. Pendry, J. B., A. J. Holden, D. Robbins, and W. Stewart, "Magnetism from conductors and enhanced nonlinear phenomena," *IEEE Transactions on Microwave Theory and Techniques*, Vol. 47, No. 11, 2075–2084, 1999.

5. Eleftheriades, G. V., O. Siddiqui, and A. K. Iyer, "Transmission line models for negative refractive index media and associated implementations without excess resonators," *IEEE Microwave and Wireless Components Letters*, Vol. 13, No. 2, 51–53, 2003.

6. Caloz, C. and T. Itoh, "Transmission line approach of left-handed (LH) materials and microstrip implementation of an artificial LH transmission line," *IEEE Transactions on Antennas and Propagation*, Vol. 52, No. 5, 1159–1166, 2004.

7. Lai, A., C. Caloz, and T. Itoh, "Composite right/left-handed transmission line metamaterials," *IEEE Microwave Magazine*, Vol. 5, No. 3, 34–50, 2004.

8. Casares-Miranda, F. P., P. Otero, E. Márquez-Segura, and C. Camacho-Peñalosa, "Wire bonded interdigital capacitor," *IEEE Microwave and Wireless Components Letters*, Vol. 15, No. 10, 700–702, 2005.

9. Márquez-Segura, E., F. P. Casares-Miranda, P. Otero, C. Camacho-Peñalosa, and J. E. Page, "Analytical model of the wire bonded interdigital capacitor," *IEEE Transactions on Microwave Theory and Techniques*, Vol. 54, No. 2, 748–754, 2006.

10. Page, J. E., E. Márquez-Segura, F. P. Casares-Miranda, J. Esteban, P. Otero, and C. Camacho-Peñalosa, "Exact analysis of the wire-bonded multiconductor transmission line," *IEEE Transactions on Microwave Theory and Techniques*, Vol. 55, No. 8, 1585–1592, 2007.

11. Goldfarb, M. E. and R. A. Pucel, "Modeling via hole grounds in microstrip," *IEEE Microwave and Guided Wave Letters*, Vol. 1, No. 6, 135–137, 1991.

12. Hoffmann, R. K., *Handbook of Microwave Integrated Circuits*, Artech House, Inc., 1987.

13. Gupta, K. C., R. Garg, I. Bahl, and P. Bhartia, *Microstrip Lines and Slotlines*, 2nd ed. Artech House, Inc., 1996.

14. Silvester, P. and P. Benedek, "Microstrip discontinuity capacitances for right-angle bends, ⊤ junctions, and crossings," *IEEE Transactions on Microwave Theory and Techniques*, Vol. 21, No. 5, 341–346, 1973.

15. Easter, B., "The equivalent circuit of some microstrip discontinuities," *IEEE Transactions on Microwave Theory and Techniques*, Vol. 23, No. 8, 665–660, 1975.

16. Neale, B. M. and A. Gopinath, "Microstrip discontinuity inductances," *IEEE Transactions on Microwave Theory and Techniques*, Vol. 26, No. 10, 827–831, 1978.

17. Hammerstad, E., "Computer-aided design of microstrip couplers with accurate discontinuity models," *IEEE MTT-S Int. Microwave Symposium Digest*, 54–56, 1981.